Agricultural and Forest Meteorology 343 (2023) 109789

Contents lists available at ScienceDirect

Agricultural and Forest Meteorology

journal homepage: www.elsevier.com/locate/agrformet

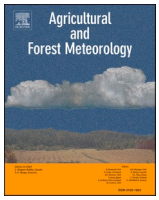

Modeling China's terrestrial ecosystem gross primary productivity with BEPS model: Parameter sensitivity analysis and model calibration

Xiuli Xing [a], Mousong Wu [a,*], Wenxin Zhang [b], Weimin Ju [a], Torbern Tagesson [b], Wei He [a], Songhan Wang [c], Jun Wang [a], Lu Hu [a], Shu Yuan [a], Tingting Zhu [a], Xiaorong Wang [d], Youhua Ran [e], Sien Li [f], Chunyu Wang [f], Fei Jiang [a,g]

[a] International Institute for Earth System Science (ESSI), Nanjing University, Nanjing 210023, China
[b] Department of Physical Geography and Ecosystem Science, Lund University, Lund 22362, Sweden
[c] Key Laboratory of Crop Physiology and Ecology in Southern China, Nanjing Agricultural University, Nanjing 210095, China
[d] School of Biological Sciences, The University of Hong Kong, Pokfulam, Hong Kong SAR 999077, China
[e] Heihe Remote Sensing Experimental Research Station, Northwest Institute of Eco-Environment and Resources, Chinese Academy of Sciences, Lanzhou 730000, China
[f] Center for Agricultural Water Research in China, China Agricultural University, Beijing 100083, China
[g] Frontiers Science Center for Critical Earth Material Cycling, Nanjing University, Nanjing 210023, China

ARTICLE INFO

Keywords:
Gross primary productivity
Ecosystem modeling
Satellite-data-driven
Global sensitivity analysis
Uncertainty analysis

ABSTRACT

Terrestrial ecosystems are the largest sink for carbon, and their ecosystem gross primary productivity (GPP) regulates variations in atmospheric carbon dioxide (CO_2) concentrations. Current process-based ecosystem models used for estimating GPP are subject to large uncertainties due to poorly constrained parameter values. In this study, we implemented a global sensitivity analysis (GSA) on parameters in the Boreal Ecosystem Productivity Simulator (BEPS) considering the parameters' second-order impacts. We also applied the generalized likelihood estimation (GLUE) method, which is flexible for a multi-parameter calibration, to optimize the GPP simulation by BEPS for 10 sites covering 7 plant functional types (PFT) over China. Our optimized results significantly reduced the uncertainty of the simulated GPP over all the sites by 17 % to 82 % and showed that the GPP is sensitive to not only the photosynthesis-related parameters but also the parameters related to the soil water uptake as well as to the energy balance. The optimized GPP across South China showed that the mix forest, shrub, and grass have a higher GPP and are more controlled by the soil water availability. This study showed that the GLUE method together with the GSA scheme could constrain the ecosystem model well when simulating GPP across multiple ecosystems and provide a reasonable estimate of the spatial and temporal distribution of the ecosystem GPP over China. We call for more observations from more sites, as well as data on plant traits, to be collected in China in order to better constrain ecosystem carbon cycle modeling and understand its response to climate change.

1. Introduction

The terrestrial ecosystem gross primary productivity (GPP), quantifying the amount of carbon (C) assimilated by plants from the atmosphere, is the largest C flux within the C cycle (Beer et al., 2010), and regulates variations of atmosphere carbon dioxide (CO_2) concentrations over the past several decades (Forkel et al., 2016; Wenzel et al., 2016). Climate change and anthropogenic activities have induced profound impacts on the terrestrial ecosystem carbon cycles by enhancing photosynthesis with the elevated atmospheric CO_2 concentrations on one hand (Wang et al., 2020) and by impeding plant growth with more frequent droughts and disturbances on the other hand (Bastos et al., 2020; Gampe et al., 2021; Orth et al., 2020; Wang et al., 2020, 2019). Therefore, accurate estimates of GPP can improve our understanding of terrestrial C dynamics (Huang et al., 2021; Running et al., 2004; Xiao et al., 2014b) and their responses to current and future climate change (Li et al., 2018).

Over the past decades, process-based ecosystem models have been developed and commonly used to understand mechanisms that regulate terrestrial C fluxes at local, regional, continental, and global scales

* Corresponding author.
E-mail address: mousongwu@nju.edu.cn (M. Wu).

https://doi.org/10.1016/j.agrformet.2023.109789
Received 21 March 2023; Received in revised form 10 October 2023; Accepted 24 October 2023

(Huntzinger et al., 2017; Piao et al., 2013; Sitch et al., 2015). The modeled GPP has been found to have large uncertainties, mainly due to uncertainties in model parameters, inputs, and structures (Beck, 1987; Zheng et al., 2018). Among those uncertainties, the uncertainties from model parameters often contribute most to the overall uncertainties of the results when climate forcing and plant functional types have been applied (Kaminski et al., 2013; Verbeeck et al., 2006; Xiao et al., 2014a). The GPP simulated by ecosystem models shows large uncertainties, mostly because sensitive parameters are assigned empirical values directly and have not been further calibrated (Knorr and Kattge, 2005; Luo et al., 2009; MacBean et al., 2022; Piao et al., 2013; Zhu and Zhuang, 2014). Thus, it is necessary to carefully take into account the parameter uncertainties in modeling ecosystem GPP. One effective tool to reduce the parameter uncertainties of process-based ecosystem models is parameter sensitivity analysis (PSA) and model calibration (Bastrikov et al., 2018; Prihodko et al., 2008; Senapati et al., 2016; Verbeeck et al., 2006; Yang et al., 2022; Zhang et al., 2019; Zhu and Zhuang, 2014). The PSA method is capable of identifying sensitive parameters to concentrate efforts on calibrating the sensitive parameters. Many PSA methods have been developed (Beven and Binley, 1992; Castaings et al., 2012; Czitrom, 1999; Metropolis and Ulam, 1949; Morris, 1991; Norton, 2015; Pianosi et al., 2015; Sobol, 1993; Tarantola et al., 2006), and can be divided into local PSA methods and global PSA methods Local PSA methods are efficient, quick and easy to use but only appropriate if the parameter uncertainties are small or the model is linear. With the increasingly complex of model structure and the relationship between model parameters, global PSA method demonstrates its ability to assess the output uncertainties across the entire parameter space and determine the interaction effects of the parameters on the output. Global PSA methods may be divided into three types: screening, regression-based and variance-based. The screening method is capable of providing parameter rankings, whereas the variance-based method is able to quantify the amount of variance that each parameter contributes to the unconditional variance of the model output (Li et al., 2009). However, the well-known shortcoming of global SA algorithm is heavy computational burden. Lu et al. (2013) proposed a two-step global PSA approach (hereafter called TS-GSA) that combined a screening global PSA method called Morris and a variance-based global PSA method called random-sampling, high-dimensional model representation (RS-HDMR). TS-GSA can be used efficiently to identify sensitive parameters as well as their interactions in ecosystem models with fewer simulations for different sets of model parameters and can be readily applied to any model with complex structure. It has been used by some process-based models to detect the sensitive parameters (Dantec-Nédélec et al., 2017; Jabloun et al., 2018; Li et al., 2020; Liu et al., 2022; Lu et al., 2013; Wu et al., 2019a).

For the parameter optimization, several methods have also been proposed, such as the data assimilation algorithms (Elbern et al., 2000; Hatfield et al., 2021; Kaminski et al., 2013; Rayner et al., 2005; Scholze et al., 2016, 2019; Wu et al., 2020a, 2019b), machine learning algorithms and the optimization approaches using the Monte Carlo sampling algorithm (Metropolis and Ulam, 1949; Verbeeck et al., 2006; Wu et al., 2020b, 2019c, 2021, 2011, 2012). Variational algorithm which is a data assimilation algorithm needs to generate the adjoint code, the computational cost often exceeds the original model runs and the development of the model needs the re-calculation of the adjoint code, which is not convenient for model applications to different situations as well as for transferring of the algorithm to different models (Altaf et al., 2013). Machine learning methods have become popular in simplifying the parameterizations of process-based models in recent years (Dagon et al., 2020; Koppa et al., 2022; Ma et al., 2022; Sawada, 2020), but its black-box nature hinders the interpretability, which is an important requirement if the influence of individual covariates needs to be realistically represented to improve process understanding (Koppa et al., 2022). With the fast development of computational capacity, the Monte Carlo-based approach is commonly used in parameter calibration. For the Monte Carlo sampling-based optimization method, it is easy to be adopted in an ecosystem model with a large number of parameters. This method allows for the assessment of nonlinear interactions between parameters with a large amount of samplings and flexible definitions of the prior parameter distributions (Beven and Freer, 2001; Franks et al., 1997; O'Neill et al., 1982; Prihodko et al., 2008).

The generalized likelihood uncertainty estimation (GLUE) is a widely used Monte Carlo sampling-based optimization and uncertainty analysis method. GLUE is based on a large number of Monte Carlo simulations with uniform distributions and then selects the acceptable parameter sets with equal modeling performance based on the criteria applied to the model outputs with respect to their performance (Beven, 2009). The core assumption of the GLUE is "equifinality", which indicates that different parameter sets can produce equally good results (Beven, 2006; Beven and Binley, 1992). Thus, the GLUE does not provide a single best fit against measurements, instead, it uses an ensemble of accepted model simulations to represent equally good results based on a criteria defined in informal likelihood measures (e.g. coefficient of determination, R^2, and root mean square error, RMSE) (Beven, 2006; Stedinger et al., 2008). This approach has been extensively used to calibrate process-based ecosystem models such as the CoupModel (Jansson, 2012; Houska et al., 2014; Khoshkhoo et al., 2015; Metzger et al., 2016; Senapati et al., 2016; Wang et al., 2022a; Wu et al., 2019a). It has been proven to efficiently deal with parameter uncertainties in highly nonlinear ecosystem models (Prihodko et al., 2008; Stedinger et al., 2008).

In this study, we implemented TS-GSA and GLUE to conduct parameter sensitivity analysis and optimization for the Boreal Ecosystem Productivity Simulator (BEPS) model using GPP observations from 10 sites in China. Few previous studies have used model-data fusion approaches to optimize parameters in BEPS for multiple sites. Most of these studies only focused on certain parameters related to the photosynthesis process such as the maximum carboxylation rate of Rubisco at the top of the canopy at 25 °C (V_{cmax25}) (Chen et al., 2017; He et al., 2017; Ju et al., 2006; Wang et al., 2021a). The sensitivity of parameters in BEPS related to different processes and their variations in different ecosystems remain unclear. Our objectives were to: (1) investigate the sensitivity of parameters in BEPS for simulating GPP across various ecosystems in China; (2) optimize the selected sensitive parameters separately for different ecosystems; and (3) evaluate the response of optimized model to climate change in China.

2. Materials and methods

2.1. BEPS model

BEPS model contains 8 plant functional types (PFTs), namely, evergreen needleleaf forests (ENF), deciduous needleleaf forests (DNF), deciduous broadleaf forests (DBF), evergreen broadleaf forests (EBF), mixed forests (Mix), shrub, grass, and crop. BEPS simulates diurnal variations in GPP using hourly meteorological data (i.e., air temperature, relative humidity, wind speed, precipitation, and solar radiation), soil texture, C pools, and vegetation parameters, including clumping index, land cover type, and daily LAI as model inputs (Fig. 1). BEPS simulates the dynamics of carbon pools beyond GPP. It stratifies the soil carbon stock into nine pools (surface structural litter, surface metabolic litter, soil structural litter, soil metabolic litter, coarse woody litter, surface microbe, soil microbe, slow, and passive carbon pools). These nine carbon pools are used to calculate heterotrophic respiration (HR) and autotrophic respiration (AR), which is used to estimate net ecosystem productivity (NEP). Since there is no turnover rate of the carbon pools in the initial stage of the simulation at the different sites, a spin-up was performed (Chen et al., 2019a, 2019b) to give an initial state to each pool and to avoid the impact on the uncertainty of the carbon balance when optimizing the GPP. Therefore, we started the simulation at the balanced C pools. The details on implementation of a

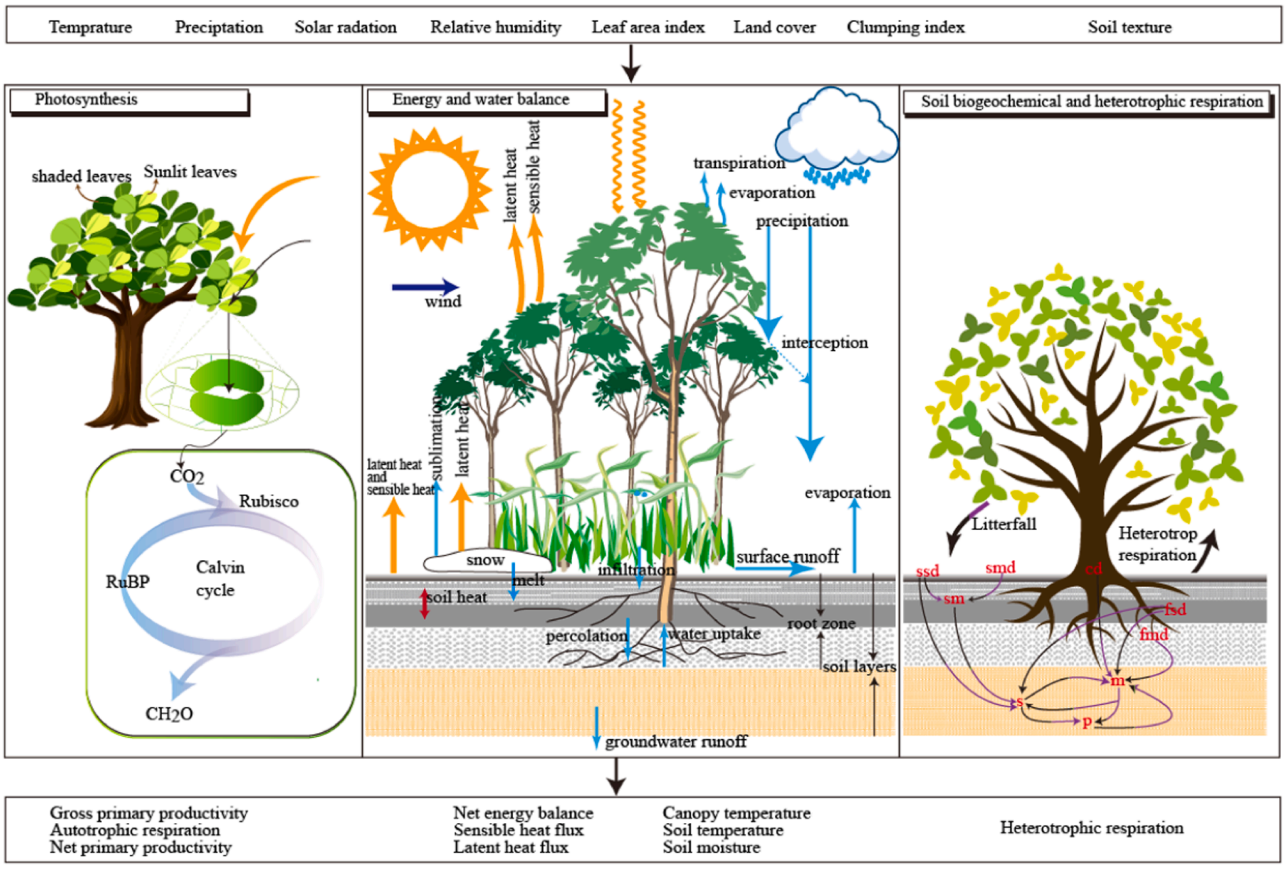

Fig. 1. The structure of the Boreal Ecosystem Productivity Simulator (BEPS) model. The yellow arrows represent the energy processes, blue arrows represent the water cycle processes, the black with purple arrows represent the carbon and nitrogen processes, black arrows are related to the carbon process. ssd: carbon and nitrogen stock in surface structural detritus; smd: carbon and nitrogen in surface metabolic detritus; sm: carbon and nitrogen in surface microbe; s: carbon and nitrogen in slow; p: carbon and nitrogen in passive; m: carbon and nitrogen in soil microbe; fmd: carbon and nitrogen stock in fine metabolic detritus. fsd: carbon and nitrogen stock in fine structural detritus. cd: carbon and nitrogen stock in the woody litter.

model spin-up can be found in Chen et al. (2019b). The BEPS model stratifies the canopy into the overstory and understory, accounting for the sunlit and shaded leaves respectively. GPP is calculated accordingly using a two-leaf (sunlit and shaded leaves) Farquhar's biochemical model (Farquhar et al., 1980) accounting for the canopy-level of carbon assimilation (Chen et al., 1999):

$$\mathrm{GPP} = GP_{sunlit}LAI_{sunlit} + GPP_{shaded}LAI_{shaded} \quad (1)$$

where GPP_{sunlit} and GPP_{shaded} are the GPP of sunlit and shaded leaves, respectively; LAI_{sunlit} and LAI_{shaded} are the leaf area indices of sunlit and shaded leaves. Beside, BEPS simulates fluxes of plant and soil C, water and energy balance at each time-step. Autotrophic respiration is separated into growth respiration and maintenance respiration components. Growth respiration is calculated as 20 % of GPP while maintenance respiration is temperature dependent. Details of the model can be found in Ju et al. (2006) and Chen et al. (2007).

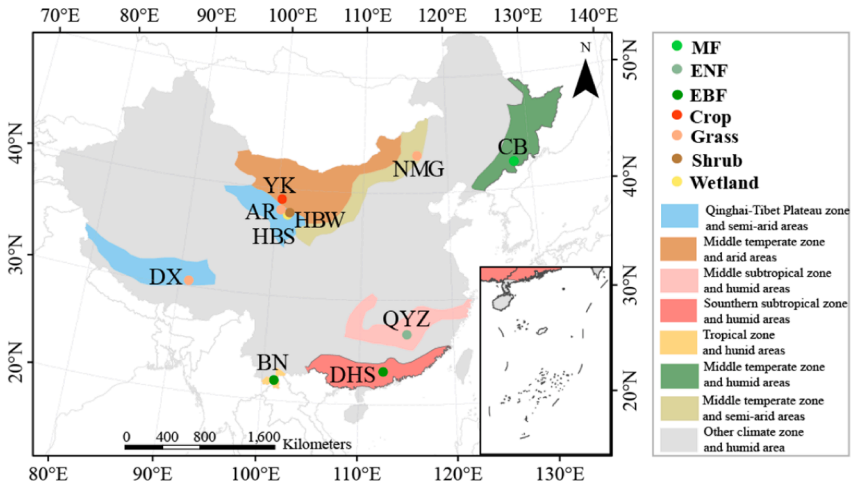

Fig. 2. The distribution of plant functional types and the locations of the 10 eddy covariance flux sites across China.

2.2. Data

2.2.1. Eddy covariance flux and meteorological measurements

We collected hourly meteorological and GPP data from 10 eddy covariance flux sites (Fig. 2). The metrological data were used to drive the model and the GPP data were used to calibrate and validate the model (Table 1). Data from 8 of the sites (spanning from 2003 to 2010) were collected from ChinaFlux (http://chinaflux.org/), and the remaining two (spanning from 2008 to 2010) were collected from the National Tibetan Plateau Third Pole Environment Data Center (Li et al., 2013). These sites are distributed in different climate zones and humid areas, defined using data from Resource and Environment Science and Data center (https://www.resdc.cn/). These 10 sites represent 7 PFTs that are typical in China, i.e. grass (3 sites), crop (1 site), shrub (1 site), evergreen broad-leaved forest (EBF, 2 sites), evergreen coniferous forest (ENF, 1 site), mixed forest (MF, 1 site), wetland (1 site). We used the 1/3 of observations for model validation and 2/3 for model calibration.

2.2.2. Leaf area index input data

We used the GLOBMAP LAI version3.0 data from 2003 to 2019 with 8-day temporal and ~0.07° LAI spatial resolution (Liu et al., 2012). Beside, the 8-day and 0.05° GLASS LAI from 2003 to 2010 and the MODIS LAI product from 2003 to 2010 (MOD15A2H) with an 8-day temporal resolution and a 500-m spatial resolution were also used to drive BEPS model. We converted the 8-day LAI into daily LAI to drive the BEPS model by assuming that the LAI between two LAI observations keep unchanged. LAI for the 10 sites was then extracted from this product at their original resolution. GLOBMAP LAI was also used for the regional simulation, we aggregated the GLOBMAP LAI (2010–2019) from 0.07° × 0.07° to 1° × 1°

2.2.3. GPP datasets

Four global GPP datasets were used in comparison with the GPP simulated by BEPS over China. The GPP datasets used were: (1) Monthly GPP at 0.5° × 0.5° from the Vegetation Photosynthesis Model (VPM) (Zhang et al., 2017). (2) Monthly GPP at 0.05° × 0.05° derived from the satellite-based near-infrared reflectance (NIRv) (Wang et al., 2021b). (3) The annual Light Response Function (LRF) GPP dataset at 0.05° × 0.05° resolution was obtained with an ecosystem-level physiological approach (Tagesson et al., 2021). (4) An 8-day GPP dataset with 0.05° × 0.05° resolution based on a revised light use efficiency model (EC-LUE) (Zheng et al., 2020). All 8-day (MODIS and EC-LUE) GPP datasets were aggregated to the monthly data sets. We kept the original spatial resolution of the GPP datasets in deriving the regional GPP over China as well as over specific parts of China.

2.2.4. Climate data for the regional simulation

The climate data used to drive the regional BEPS simulation were derived from ECMWF Reanalysis Atmospheric 5th Generation (ERA5) (Hersbach et al., 2020). The input variables included hourly air temperature, solar radiation, relative humidity, wind speed, and precipitation from 2010 to 2019 at 1° × 1° resolution.

2.2.5. Crop management data

Corn is the main grain crop type of the Yingke (YK) site (Li et al., 2009; Wu et al., 2019a). In 2008, it was hole seeded on April 20 and harvested on September 22. There were five irrigation events throughout the growth period (May to September), and in total irrigation added 885 mm (Wang et al., 2013). For convenience we added the daily irrigation to the precipitation of the same day in BEPS to consider irrigation practice.

2.2.6. SPEI

The standardized precipitation evapotranspiration index (SPEI) can be used for determining the onset, duration, and magnitude of drought conditions. Values of SPEI less than −0.5 correspond to mild drought, less than −1 to moderate drought, less than −1.5 to severe drought, and less than −2 to extreme drought. Here, we used the 0.5° × 0.5° SPEI3 spanning from 2010 to 2018 (https://spei.csic.es/) to study the sensitivity of GPP simulations to drought.

2.2.7. LT_SIF

The 0.05° × 0.05° long-term consistent global solar-induced chlorophyll fluorescence (LT_SIF) data (Wang et al., 2022b) was also used in this study. This SIF dataset spans the period from July 1995 to December 2018, here we used the data from 2010 to 2018. We re-gridded the LT_SIF into 0.5° × 0.5° to calculate the correlation with SPEI.

2.3. Parameter sensitivity analysis and optimization

In this study, TS-GSA method and GLUE optimization approach were implemented into BEPS (Fig. 3), as summarized below:

(1) Parameters selection. We selected parameters that were potentially relevant to energy and water balance, as well as autotrophic and heterotrophic respiration based on the mechanistic understanding of the BEPS model. In total, 21 parameters were selected for the sensitivity analysis based on prior knowledge (Table 2) (Bonan et al., 1993; Chen et al., 2007, 1999; He et al., 2014; Ju et al., 2006, 2010).
(2) Parameter sensitivity analysis: Morris & RS-HDMR. We conducted global parameter sensitivity using the TS-GSA proposed by Lu et al. (2013). Using the selected parameters from step (1), the Morris method (Morris, 1991) was first used to rank the potentially sensitive parameters. Furthermore, we used the RS-HDMR method (Ziehn and Tomlin, 2008) to quantify the interactions between parameters and re-rank parameter sensitivities before deriving the sensitive parameters for calibration.
(3) Parameter calibration. We used the GLUE approach to calibrate the sensitive parameters from step (2) by randomly sampling the parameter values within their respective prior ranges for 10,000 times with uniform distribution to realize the model space. We

Table 1
Information of 10 flux sites used in this study. The annual total precipitation (P) and annual mean temperature (T) are given based on the available observations. PFT stands for plant functional type. MF is mixed forest, EBF is evergreen broadleaf forest, and ENF is evergreen needleleaf forest.

Site Name	Lat (°N)	Lon (°E)	P (mm)	T (°C)	PFT	Calibration years	Validation years
Arou (AR)	38.05	100.45	349.45	−0.1	Grass	2008~2009	2010
Changbaishan (CB)	42.40	128.10	234.33	3.65	MF	2003~2008	2009~2010
Dangxiong (DX)	30.50	91.07	220.85	2.72	Grass	2004~2008	2009~2010
Dinghushan (DHS)	23.17	112.53	729.09	20.12	EBF	2003~2008	2009~2010
Haibei Shrub (HBS)	37.67	101.33	236.33	−1.26	Shrub	2003~2008	2009~2010
Haibei Wetland (HBW)	37.61	101.33	236.33	−1.26	Wetland	2003~2008	2009~2010
Neimenggu (NMG)	43.33	116.40	80.06	1.38	Grass	2004~2008	2009~2010
Qianyanzhou (QYZ)	26.74	115.06	583.70	17.74	ENF	2003~2008	2009~2010
Xishuangbanna (BN)	21.93	101.27	737.1	19.40	EBF	2003~2008	2009~2010
Yingke (YK)	38.85	100.42	31.71	7.40	Crop	2008~2009	2010

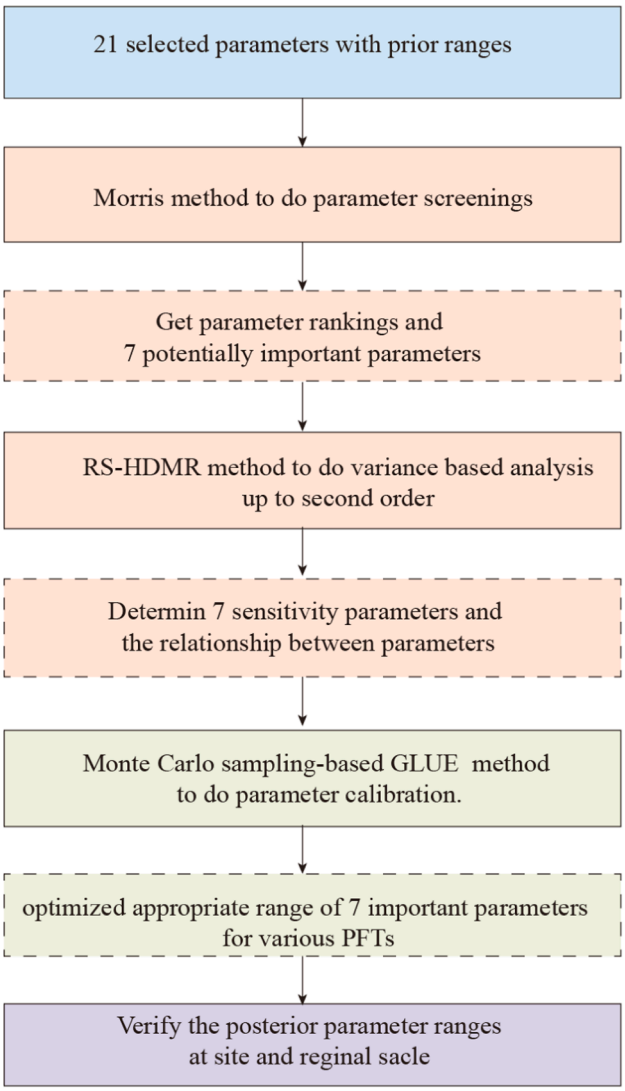

Fig. 3. Flowchart of the methodology for the parameter sensitivity analysis and model calibration of the BEPS model in this study.

then separately took the best 100 sets of parameters (acceptance ratio of 1 %) with the lowest RMSE as the optimized parameter sets called posterior parameters.

(4) Model validation. The outputs of GPP simulated by the 100 optimized parameter sets selected with the best 100 RMSEs were then compared with the observed GPP to evaluate the goodness of parameter optimization in the validation years.

2.3.1. Parameter selection

The 21 model parameters selected to four processes in the BEPS model were related (Table S1): photosynthesis (V_{cmax25}, m_{H_2O}, N_{leaf}, b_{H_2O}, $m_{V_{cmax,N}}$, b_{CO_2}), energy and water balance (b, K_{sat}, f_{leaf}, r_{decay}, sr_{min}, h_o,h_u d_{root}, A_{vo}, A_{no}, A_{sat}, A_{dry}, r_{dra}), heterotrophic respiration (d_{litter}) and autotrophic respiration (Q_{10}). Thirteen of the parameters (V_{cmax25}, m_{H_2O}, N_{leaf}, $m_{V_{cmax,N}}$, b, K_{sat}, r_{decay}, sr_{min}, h_o,h_u d_{root}, A_{vo}, A_{no},) have PFT-specific values, and the remaining eight (b_{H_2O}, b_{CO_2}, f_{leaf}, A_{sat}, A_{dry}, r_{dra}, Q_{10}, d_{litter}) have common values for all PFTs. All selected parameters were given a prior range based on the default value of the model. Since the 21 parameters selected above are all empirical values in the BEPS model, a prior ranges of the parameters were initially used as the default values for each parameter minus and plus the corresponding values multiplied by 25 %. The ranges of r_{decay}, K_{sat} and d_{root} have been changed after constant experimentation and consideration of the meaning of the parameters. r_{decay} calculates the proportion of roots distributed in the soil with a determined prior range of minus or plus 10 % of the default parameter value and the maximum is 1. K_{sat} is the saturated hydraulic conductivity of the soil with a range of minus or plus 75 % of the default parameter value. d_{root} is the root depth with the minimum range defined as the default value minus the corresponding value multiplied by 25 %, and maximum range is the default value plus the corresponding value multiplied by 50 %.

2.3.2. TS-GSA method

Morris is a derivative-based method to implement a global parameter sensitivity analysis (Morris, 1991). When ranking all selected model parameters by their elementary effects on the model output, the higher a parameter is ranked, the more sensitive the model output is to that specific parameter. Thus, we can identify important parameters for calibration.

As the Morris method cannot distinguish the interactions between parameters, we therefore needed to apply the RS-HDMR method to identify the interactions between parameters for those parameters selected in the Morris step. The RS-HDMR method can calculate the first-order sensitivity to measure the effect of parameter on the model output, and the second-order sensitivity to measure the contribution of the interaction effect of parameters. Therefore, the RS-HDMR method not only verifies the parameter-screening results by the Morris method but also provides additional information about the interactions among parameters. Details of RS-HDMR method can be found in Lu et al. (2013), and the software package to implement this method is freely available in Ziehn and Tomlin (2009).

Table 2
Prior and posterior (bold font) values of selected sensitivity parameters. The posterior ranges were the minimum and maximum of the 100 parameter sets.

Parameters	V_{cmax25}	m_{H_2O}	N_{leaf}	$m_{V_{cmax,N}}$	b_{H_2O}	r_{decay}	f_{leaf}
Grass	30.00 ± 7.50	4.00 ± 1.00	2.70 ± 0.67	0.57 ± 0.14	0.02 ± 0.01	0.95 ± 0.10	0.50 ± 0.13
	32.58 (22.76~37.48)	**4.35 (3.03~5)**	**2.94 (2.03~3.37)**	**0.63 (0.43~0.71)**	**0.02 (0.01~0.02)**	**0.92 (0.86~0.99)**	**0.49 (0.38~0.62)**
crop	36.00 ± 9.00	4.00 ± 1.00	2.38 ± 0.67	0.31 ± 0.08	0.02 ± 0.01	0.95 ± 0.10	0.50 ± 0.13
	42.56 (37.17~44.97)	**4.53 (3.22~5.00)**	**2.74 (2.25~2.96)**	**0.36 (0.30~0.39)**	**0.02 (0.01~0.02)**	**0.92 (0.86~0.99)**	**0.54 (0.39~0.62)**
Shrub	34.71 ± 7.29	8.00 ± 2.00	2.70 ± 0.67	0.57 ± 0.14	0.02 ± 0.01	0.95 ± 0.10	0.50 ± 0.13
	41.12 (33.19~43.38)	**8.85 (6.60~9.99)**	**3.16 (2.49~3.37)**	**0.67 (0.57~0.71)**	**0.02 (0.01~0.02)**	**0.90 (0.86~0.99)**	**0.56 (0.39~0.62)**
Wetland	89.45 ± 22.36	8.00 ± 2.00	2.70 ± 0.67	0.60 ± 0.15	0.02 ± 0.01	0.95 ± 0.10	0.50 ± 0.13
	72.90 (67.09~88.15)	**7.23 (6~9.97)**	**2.24 (2.02~2.84)**	**0.49 (0.45~0.61)**	**0.02 (0.01~0.02)**	**0.93 (0.86~0.99)**	**0.43 (0.38~0.57)**
EBF	39.10 ± 9.78	8.00 ± 2.00	2.97 ± 0.74	0.48 ± 0.12	0.02 ± 0.01	0.97 ± 0.10	0.50 ± 0.13
	38.01 (29.45~48.87)	**7.96 (6.02~9.89)**	**2.87 (2.24~3.70)**	**0.46 (0.36~0.60)**	**0.02 (0.01~0.02)**	**0.94 (0.87~1.03)**	**0.49(0.38~0.62)**
ENF	32.50 ± 8.13	8.00 ± 2.00	4.45 ± 1.11	0.33 ± 0.08	0.02 ± 0.01	0.95 ± 0.10	0.50 ± 0.13
	36.98 (30.75~40.48)	**8.14 (6.01~9.94)**	**4.94 (3.99~5.54)**	**0.37 (0.30~0.41)**	**0.02 (0.01~0.02)**	**0.93 (0.85~0.99)**	**0.41 (0.38~0.46)**
MF	33.00 ± 8.25	8.00 ± 2.00	3.50 ± 0.88	0.47 ± 0.12	0.02 ± 0.01	0.96 ± 0.10	0.5 ± 0.13
	35.94 (27.59~41.02)	**8.53 (6.24~9.98)**	**3.89 (3.12~4.37)**	**0.51 (0.40~0.59)**	**0.02 (0.01~0.02)**	**0.93 (0.86~0.99)**	**0.59 (0.51~0.62)**

2.3.3. Parameter calibration

The GLUE method involves a large number of model runs, each of which is driven by randomly selected input parameter values drawn from uniform prior distributions across the range of each parameter. In this study, we first assumed that all parameters conform to the uniform distribution, then randomly sampled 10,000 times from input distributions for every sensitive parameter selected from TS-GSA method. After transforming back to their actual values, run the BEPS model. The performance of each run is thereafter taken as behavioral or non-behavioral based upon the comparison of simulated versus observed data. Model runs that meet specified acceptability criteria are received as behavioral runs, otherwise are rejected as non-behavioral and removed them from further analysis. A total of 10,000 simulations were performed based on the Monte Carlo sampling from the parameters which were selected from TS-GSA. These 10,000 simulations with the present BEPS setup represents a balance between computational limitation and maximizing coverage of the parameter space. Out of these runs, 100 behavioral runs were selected using evaluation criteria (root mean square error, RMSE) by comparing the model outputs with measured data for ten sites.

The extent to which parameters were constrained by the observations can be identified by comparing the difference between the cumulative distribution of frequency (CDF) of prior and posterior parameters. We assumed that the prior distribution is uniform, so the CDF of the 10,000 sets of prior parameters is a regular diagonal shape, while the CDF of the 100 sets of posterior parameters will have a corresponding shape according to the corresponding parameter combination. When the CDF of posterior parameters differ substantially from their prior uniform distributions, their range ratios (i.e. posterior parameter range divided by prior parameter range) will become smaller. Parameters with range ratios lower than 0.6 were selected as very well constrained (Zhang et al., 2019).

2.3.4. Model validation

The 100 sets of parameters derived from the calibration period using the GLUE method were used to run the BEPS model to obtain the ensemble daily GPP simulations of validation years. The observed daily GPP from the validation years of each site was used to evaluate the reliability and extrapolation of the posterior parameters identified in calibration. With the constrained parameters, we took the mean of each posterior parameter ensemble as the optimal value and ran the model to obtain the regional GPP simulations. The other global GPP datasets collected in this study were used to compare with the regional prior and posterior GPP distributions. We calculated the GPP of China from 2010 to 2016 using the prior and posterior parameters forced by GLOBMAP LAI product and compared with referenced GPP products.

3. Results

3.1. Parameter sensitivity over plant functional types

We found that GPP is most sensitive to four parameters, i.e. r_{decay}—a parameter related to soil water availability (SWA), $V_{cmax}25$, $m_{V_{cmax,N}}$, N_{leaf}—parameters related to photosynthesis. The latter three parameters basically had the same relative importance for all sites (Fig. 4a). The ranking of photosynthesis and SWA relevant parameters generally differed between PFTs. For the crop site (YK), the averaged relative importance of the photosynthesis relevant parameters is 0.23, while for the SWA relevant parameters it is 0.08. We found that at the ENF site (QYZ), photosynthesis and SWA relevant parameters have the similar relative importance to the YK site. While for the shrub (HBS), wetland (HBW) and MF (CB) sites, the sensitivity of SWA relevant parameters is a little higher than the photosynthesis relevant parameters.

We also noticed the differences in the relative importance of parameters over grassland ecosystems. For alpine grassland (i.e. AR and DX), photosynthesis relevant parameters are more important (0.21) than the SWA relevant parameters (0.11). While for the semi-arid grassland NMG site the GPP shows more sensitive to the SWA relevant parameters, with the relative importance of r_{decay} in NMG of 0.35, followed by the mean relative importance value of 0.14 from the photosynthesis relevant parameters. For the two EBF sites (BN and DHS), the sensitivity of the parameters also shows to be different. The tropical rainforest from the BN site is most sensitive to soil hydrology, with the relative importance of the SWA relevant parameters (0.30) larger than the mean relative importance of the photosynthesis relevant parameters (0.16). Conversely, for the subtropical monsoon DHS site, photosynthesis relevant parameters are shown to be more sensitive, with the mean relative importance of 0.20 and the SWA relevant parameters have the relative importance of 0.15.

The sensitivity index calculated from the RS-HDMR (Fig. 4b) is generally consistent with the Morris sensitivity results (Fig. 4a). For the crop site YK, the three parameters i.e. $V_{cmax}25$, N_{leaf}, $m_{V_{cmax,N}}$ account for 89.27 % of the total normalized parameter sensitivity. While for the other sites, the most sensitive parameters are r_{decay}, $V_{cmax}25$, N_{leaf}, and $m_{V_{cmax,N}}$, and they contribute to more than 80 % of the parameter sensitivity. The first-order effects of all remaining parameters together and the total second-order effects of parameters are relatively small but show not negligible in their contribution to the GPP simulation.

3.2. Posterior parameter distributions

The posterior distribution of the sensitive parameters shows that

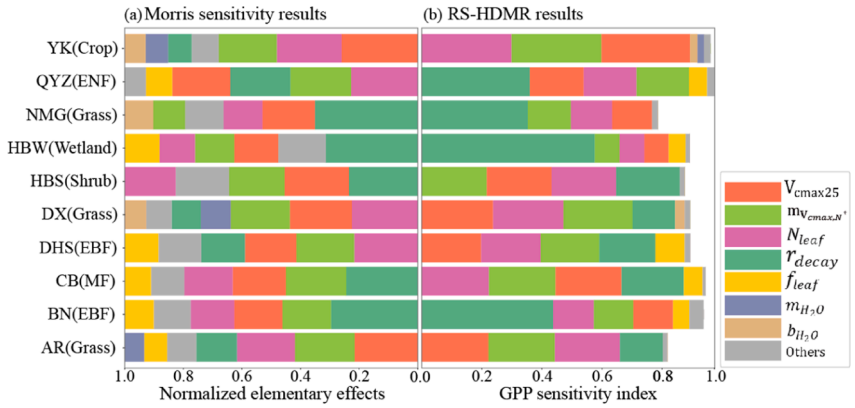

Fig. 4. The sensitivity of parameters. a, Results of Morris sensitivity analysis. The relative contribution of normalized elementary effects of different most important parameters that β value lager than 0.85 across 10 sites (colored). "others" represent the remaining unimportant parameters (gray). b, Results of RS-HDMR analysis. First-order GPP sensitivity indices of most important parameters for all sites (colored). "others" represent the interactions (second-order effects) among parameters (gray).

they are constrained well with the GLUE approach (Fig. 5), and the posterior ranges of parameters differ among sites (Table 2). Overall, the posterior range ratio (the ratio of posterior parameter range to the prior parameter range) of the sensitive parameters varied from 0.14 to 0.99.

We noticed that the sensitive parameters V_{cmax25}, N_{leaf}, and $m_{V_{cmax,N}}$ from all 10 sites are efficiently constrained at most sites, but they depict different posterior ranges in different climate zones. For example, the parameter range ratios for V_{cmax25}, N_{leaf}, and $m_{V_{cmax,N}}$ at the alpine

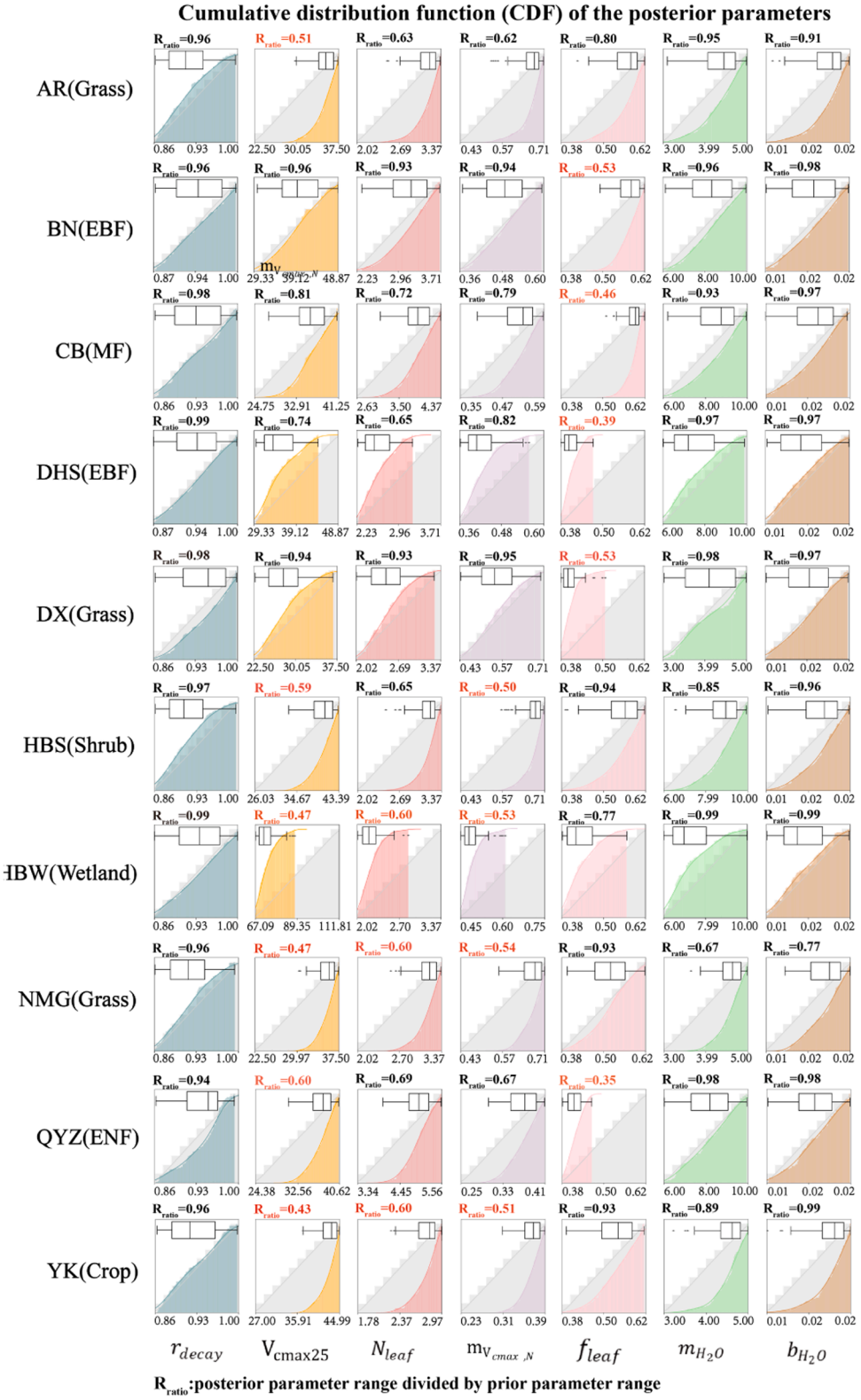

Fig. 5. The cumulative distribution functions (CDF) of posterior parameters after calibration. Lightered gray color denotes the prior CDF distributions, colored denote the posterior CDF distributions. Boxplot denotes the posterior mean, 1st and 3rd quantiles, and the error bar denotes the minimum and maximum values, scatter denotes the outlier. The red R_{ratio} was the parameters with range ratios lower than 0.6.

grassland AR site are 0.51, 0.63, and 0.62 respectively, and their posterior CDF distributions are all centered on the right-hand side of the prior range. Accordingly, the semi-arid grass site NMG depict similar posterior range ratios for the three parameters (0.47, 0.60, and 0.54) to the AR site. While for the alpine grass site DX these three parameters show much larger posterior range ratios (0.94, 0.87 and 0.91).

For the two evergreen broadleaf forest sites BN and DHS, we noticed quite different posterior range ratios for the parameters $V_{cmax}25$, N_{leaf}, and $m_{V_{cmax\,N}}$. The DHS site exhibits a better constraint than BN with range ratios of 0.74, 0.65, and 0.82 for $V_{cmax}25$, N_{leaf}, and $m_{V_{cmax\,N}}$, respectively. While at BN, their posterior range ratios are 0.96, 0.93, and 0.94, respectively. The evergreen needleleaf forest site QYZ and the mix forest site CB are shown efficiently constrained, with range ratios of 0.60, 0.69, 0.67 for the three parameters $V_{cmax}25$, N_{leaf}, and $m_{V_{cmax\,N}}$ at QYZ and of 0.81, 0.72, 0.79 for them at CB. For the two Haibei sites located in the alpine climate, they are constrained relatively well with posterior range ratios of 0.59, 0.65, and 0.50 for $V_{cmax}25$, N_{leaf}, and $m_{V_{cmax\,N}}$, respectively at HBS; and posterior range ratios of 0.47, 0.60, and 0.53 at HBW. The crop site YK exhibits good constraints with posterior range ratios of 0.43, 0.60, and 0.51 for $V_{cmax}25$, N_{leaf}, and $m_{V_{cmax\,N}}$, respectively.

The parameter r_{decay}, describing the relative soil water availability for plants, is weakly constrained at all PFTs, with the posterior range ratio value larger than 0.9. While the f_{leaf} shows a good constraint in all forest EBF (BN, DHS), MF (CB), and ENF (QYZ) (range ratios: 0.53, 0.39, 0.46, and 0.35). For the EBF, the posterior CDF distribution is clustered on the right-hand side of prior range in the BN site, but focused on the left-hand side in the DHS site. With the range ratio greater than 0.6, the constraint on the parameter f_{leaf} in the forest sites outperforms the other PFTs. The semi-arid grass site NMG is shown more tightly constrained than other sites for the two parameters m_{H_2O}, b_{H_2O}, with the posterior range ratios of 0.67 and 0.77.

3.3. Validation of the optimized model

As shown in Fig. 6a, using the optimized 100 parameter sets improved the accuracy between the modeled and observed GPP (mean R^2 increases by 0.01 to 0.07, mean RMSE reduces by 0.04 to 1.7 gC m^{-2} d^{-1} as well as significantly lowered the uncertainty of the simulated GPP (standard deviation of RMSE reduces by 0.04 to 0.92 gC m^{-2} d^{-1}, standard deviation of R^2 reduces by ~0.01–0.09, see Table S2), during both the calibration and validation periods. The posterior parameters maintain the consistent performance in simulating GPP over the calibration (R^2: 0.35 to 0.92; RMSE: 0.39 to 2.54 gC m^{-2} d^{-1}) and validation periods (R^2: 0.34 to 0.93 and RMSE: 0.40 to 1.78 gC m^{-2} d^{-1}). In general, the prior model tends to underestimate GPP at AR (grass), BN (evergreen broadleaf forest), CB (mix forest), HBS (shrub), QYZ (evergreen needleleaf forest), and YK (crop) sites and overestimate GPP at DHS (evergreen broadleaf forest) and HBW (wetland) sites (Fig. 6b). With the GLUE approach, the underestimation or overestimation of GPP has been efficiently corrected with optimized parameters with the RMSE reduced by 13.74 gC m^{-2} $month^{-1}$ to 34.5 gC m^{-2} $month^{-1}$).

Due to the lacking of observation based relationship between GPP and SPEI, we use the relationship between SIF and SPEI to prove the optimization results. From Fig. S1, the distribution of correlation between posterior GPP and SPEI was similar to SIF and SPEI, which indicates the validity of our optimized results. The correlation between posterior GPP and the drought index SPEI is positive in most parts of China, especially in the northeast, east and southwest (Fig. 7a). Beside, the difference between the correlations of posterior and prior to SPEI (Δr) was positive in northern and northwestern China, which are arid and semi-arid regions of China (Fig. 7b). In central Inner Mongolia, central and western Tibet and northwestern Xinjiang we achieved Δr of 0.05, indicating improved responses to drought with the posterior parameters. For forest (ENF, EBF and Mix) and shrub, the Δr was less than 0, while the mean Δr was larger for grasslands. We further studied the Δr of grass (Fig. 7c), and its distribution (Fig. 7d). We found that for areas with the higher proportion of grass, the higher the Δr, indicating the improved grass response to drought by the posterior simulations.

4. Discussion

4.1. Parameter uncertainty

We noticed that five of the selected sensitive parameters are related to photosynthesis. $V_{cmax}25$ is the leaf maximum Rubisco capacity at the top of the canopy at 25 °C. N_{leaf} is the leaf nitrogen content at the top of the canopy. $m_{V_{cmax\,N}}$ is defined as the ratio of measured Rubisco capacity to leaf N. In BEPS, these are used to calculate the maximum photosynthetic carboxylation rate for sunlit and shaded leaves in the calculation

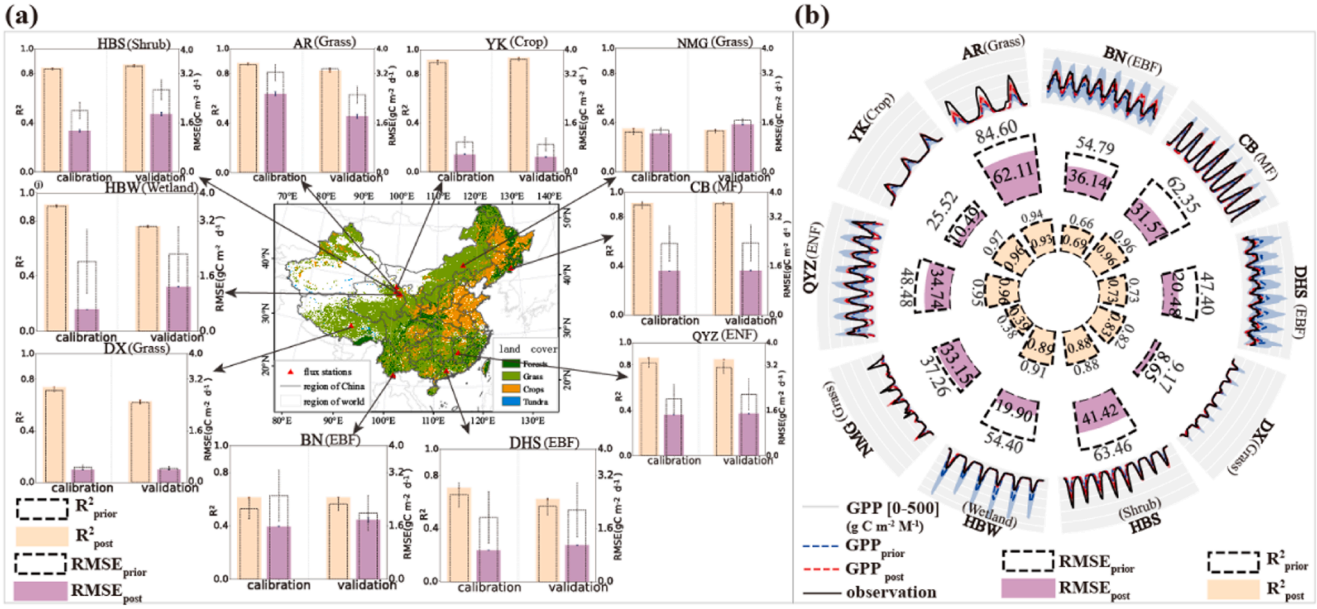

Fig. 6. The daily and monthly results of parameter calibration. a, The bar plot of R^2 and RMSE in calibration and validation periods respectively with daily GPP. b, Comparisons between prior, posterior GPP and observations with monthly GPP.

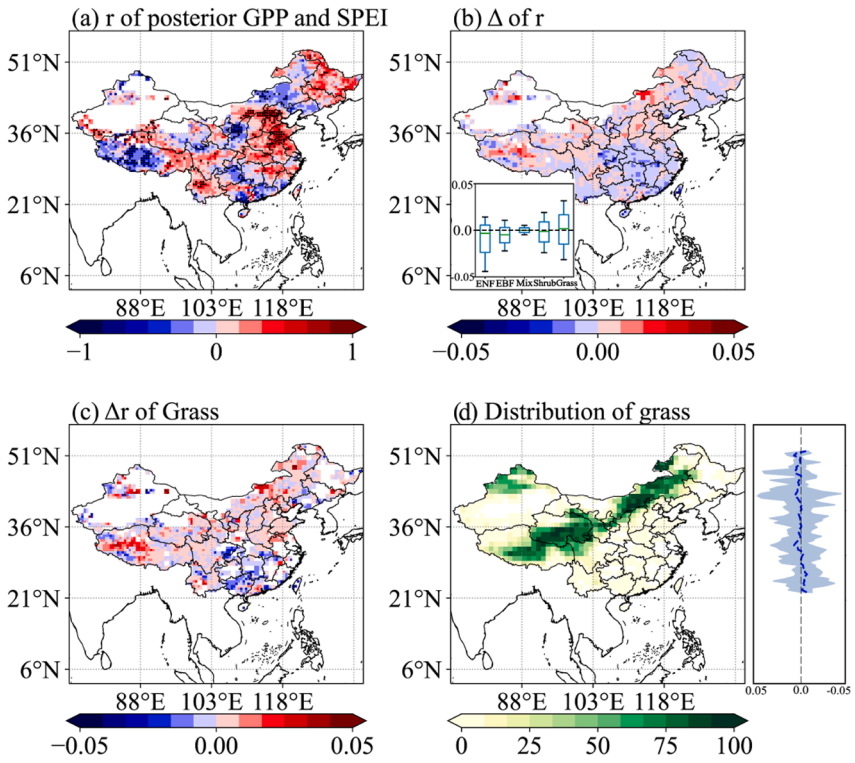

Fig. 7. Model performance in representing the vegetation response to drought during 2010 to 2018. (a) The distribution of correlation between posterior GPP and drought (SPEI<−1) (r). (b) The distribution of the difference (Δr) between the correlation of posterior gross primary productivity (GPP) with SPEI and the correlation of prior gross primary productivity (GPP) with SPEI. The insets in panel b shows the box plot of Δr in ENF, EBF, Mix, Shrub and Grass. (c) The spatial patterns of Δr for grass. (d) The proportion distribution of grass types in China. The response sensitivity summarized by latitude is shown in the right of panel d.

of net photosynthesis. These three parameters were identified as the most important parameters related to carbon uptake of vegetation (Ju et al., 2010; Mo et al., 2008; Zhou et al., 2013; Zhu et al., 2009). Therefore, their variations can cause larger changes in GPP. The m_{H_2O} and b_{H_2O} are the slope and intercept of the Ball-Berry equation (BWB model) respectively. The leaf stomatal conductance is estimated from the photosynthesis rate assuming that they have a linear relationship (Ball et al., 1987). The parameter r_{decay} is related to soil water availability (SWA). It is used to calculate the fraction of roots in the soil for each soil layer associated with the soil water availability and root water uptake (Ju et al., 2006). It is used to directly calculate the soil water stress factor and adjust the stomatal conductance. Since the soil water stress was found to vary rapidly in response to soil water dynamics in the root zone (Vicente-Serrano et al., 2013), r_{decay} affects the calculation of photosynthesis rate by influencing the stomatal conductance of vegetation. f_{leaf} controls the radiation incident on leaves.

For grass sites (AR, DX, NMG), photosynthesis parameters were more sensitive than other parameters at sites on alpine grassland in Qinghai-Tibetan Plateau (AR and DX), while r_{decay} is the most sensitive parameter when simulating semi-arid grassland (NMG). Alpine grassland in Qinghai-Tibetan Plateau (AR and DX) has low temperature, and temperature is the main limiting factor (Seddon et al., 2016). The semi-arid grassland site (NMG), which is located at Inner Mongolia in China, was shown with the decreasing trend in precipitation and indicated with a drier climate, so GPP is more sensitive to soil water. Our results are consistent with (Liu et al., 2018a) that the moisture being the major limiting factor in Inner Mongolia while grasslands in Tibetan Plateau are much more limited by thermal conditions. We noticed that the three sites in tropical and subtropical regions (BN, DHS, and QYZ) show sensitive parameters from different processes. In BN, a tropical rainforest site where there was a forest clearance between 1976 and 2003 (Qiu, 2010), the trees are very young and the growth requires much water. Beside, previous studies indicated that tropical rainforests respond to climate variability intensely (Seddon et al., 2016), therefore, occasional droughts may bring water stress to the local ecosystems and suppress GPP increase. This can explain why the SWA parameter r_{decay} is more sensitive than the photosynthesis parameters at this site, but GPP simulation from the DHS and QYZ sites are more sensitive to photosynthesis parameters. GPP in the YK site with Crop is also most sensitive to photosynthesis parameters, and the main reason is probably that corn is the main grain crop type in YK, and C4 plants have less photorespiration, higher photosynthesis efficiency, and relatively higher sensitivity to V_{cmax25} (He et al., 2021; Massad et al., 2007). For the Haibei shrub (HBS) and wetland (HBW) sites on the northeastern Tibetan Plateau in China, they have strong solar radiation with long, cold winters and short, cool summers, and are underlain by high-altitude permafrost. Beside, the roots of vegetation at HBS (shrub) and HBW (wetland) mainly exist on the top soil (0–20 cm). Due to the permafrost degradation caused by rapid climate warming, they may have lower water tables (Cheng and Wu, 2007), and these changes in the soil hydrological conditions may further affect root water uptake and make them more sensitive to moisture conditions.

Previous studies on the BEPS model's parameters mainly focused on V_{cmax25} (Chen et al., 2017; He et al., 2017; Ju et al., 2006; Wang et al., 2021a), a parameter related to photosynthesis, and largely ignored the effects of other processes on GPP. The GPP is not only affected by the photosynthesis processes, but also by the energy balance, water, temperature, and nutrients. Because the tight coupling of water, energy, and carbon (Maxwell and Condon, 2016; Migliavacca et al., 2021; Seddon et al., 2016), it is therefore important to take into account the parameters both related to photosynthesis like V_{cmax25} as well as related to water and energy when simulating GPP. Our study has shown that it is vital to comprehend the coupling mechanism of water-energy-carbon in the BEPS model before choosing an appropriate range of parameters for various PFTs.

Most process-based models use an empirical function was used to

represent the impact of plant water limitation on photosynthesis. This empirical representation can introduce significant uncertainty in simulating terrestrial carbon cycle. Trugman et al. (2018) point that soil moisture-limited productivity across models represented a large and uncertain component of the simulated carbon cycle, comparable to 3 %–286 % of current global productivity. Approximately 40–80 % of the inter-model variability was due to the functional form of the limitation equation alone. In BEPS model, r_{decay} was used to calculate a soil water stress factor (f_w), which is used to modify the slope of original BWB model linearly to include the important influence of soil water on stomatal conductance. f_w cannot capture widely documented differences in vulnerability to soil moisture stress across PFTs and rarely tested based on soil moisture (Xu et al., 2016). This soil moisture related parameter uncertainty can cause huge uncertainty of BEPS model simulations. In this study, GPP showed high sensitivity to soil moisture-related parameters but did not show good performance in constraining with observations of GPP, suggesting that the parameter needs to be further constrained using observations of moisture-related processes such as evapotranspiration.

4.2. GPP simulation uncertainties across and within different PFTs

The correlations between the posterior parameters and the performance metrics (RMSE and R^2) of the GPP show that the posterior parameter uncertainties have an effect on the model's performance (Fig. 8a and b). These two metrics represent model performance from different aspects, i.e. R^2 for dynamics and RMSE for mean of error between model and measurements. If a parameter shows correlation

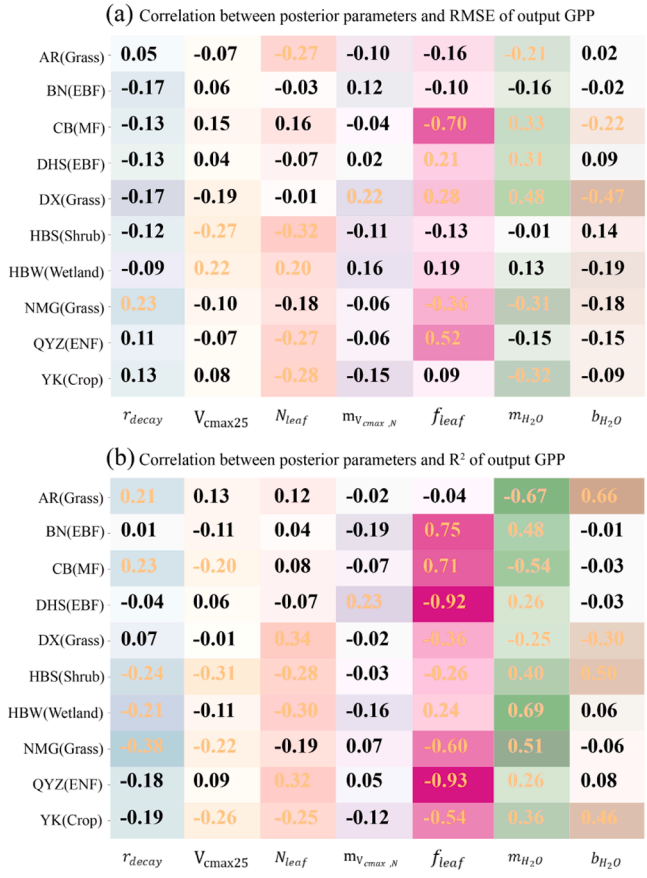

Fig. 8. The correlations matrix between posterior parameters and performance indicators (RMSE and R^2) of output GPP. Different color represents different parameter. The darker of the color, the stronger of the correlation. The fingers in the graph indicate the correlation coefficient, and correlation coefficients larger than 0.2 are highlighted in yellow.

coefficient to model performance metrics with absolute value larger than 0.2, it is assumed influential to the model performance. We noticed that the energy related parameter f_{leaf} and the leaf stomatal conductance related parameter m_{H_2O} have significant impacts on the model performance at most PFTs, indicating that the energy and stomatal processes are quite uncertain in the modeling of water-energy-carbon coupling and the leaf energy balance and leaf stomatal conductance need to be carefully calibrated when a good GPP simulation is to be achieved. The soil water availability for plants related parameter r_{decay} and photosynthesis related parameter V_{cmax25}, N_{leaf}, and b_{H_2O} show strong but diverse impacts on GPP. These three parameters show stronger correlations with the model output's R^2 at more sites compared with RMSE, indicating that they are primarily impacting the simulated dynamics of GPP.

The uncertainties in simulating GPP can also originate from the input data uncertainties because the satellite-derived LAI can also have large uncertainties due to the different input surface reflectance, retrieval algorithms, and the treatment of vegetation types (Fang et al., 2012; Liu et al., 2018b; Xie et al., 2019). Our results show that there are some systematic discrepancies between posterior simulations and measurements at AR (alpine grass), NMG (semi-arid grass). Beside, we found that the GPP exhibits an underestimation during the winter at the QYZ (ENF) site. Those discrepancies seen at those sites may be the result of the GLOBMAP LAI product's poor performance over some regions (Richardson et al., 2012). To evaluate the input data uncertainty from LAI, we also used the MODIS and GLASS LAI for parameter calibration and discovered that the MODIS-derived GPP performs better than the GLOBMAP at the AR (alpine grass, posterior R^2: 0.96, posterior RMSE: 23.50 gC m^{-2} $month^{-1}$) and NMG (semi-arid grass, posterior R^2: 0.56, posterior RMSE: 26.83 gC m^{-2} $month^{-1}$) sites (Fig. S2). Furthermore, the GLASS-derived GPP corrects the severe underestimation by GLOBMAP-driven GPP in 2010 at NMG (semi-arid grass) site and the underestimation of winter at QYZ (ENF) site (Fig. S3).

4.3. Comparisons of three LAI products

We used three LAI products to drive the posterior simulations over the 10 sites and detected the uncertainties in the input data. Overall, GPP simulations forced with GLASS had higher accuracy than simulations forced with GLOBMAP and MODIS at forest sites, while MODIS had higher accuracy than GLASS and GLOBMAP at the Tibetan-Plateau and NMG sites (Fig. 9). Furthermore, the performance of the simulations differed substantially for these three types of LAI data at some sites. We found that the seasonality of the simulated GPP was the same as the LAI data, indicating that the LAI data controls the phenology of the BEPS model. For example, at the BN site, the LAI of MODIS had double peaks (Fig. S2), and the simulated GPP thereby also showed double growing seasons (RMSE=55.27 gC m^{-2} $month^{-1}$). This did not match the single peaks of the GPP observations. However, for the LAI data of GLOBMAP and GLASS had single peak per year, and the simulated GPP was in good agreement with the observed GPP (GLOBMAP: RMSE=39.08 gC m^{-2} $month^{-1}$; GLASS: RMSE=32.87 gC m^{-2} $month^{-1}$). For the three sites at Tibet-Plateau (AR, HBS, HBW) and NMG site), MODIS LAI showed better performance than GLOBMAP and GLASS, and the underestimation of GPP values at the peak of the growing season was substantially reduced. In general, we demonstrated that GLOBMAP was the most comprehensive LAI data performing relatively well at all sites.

4.4. Caveats and implications for ecosystem modeling

In this study, the use of *in-situ* data is shown capable in well constraining both the photosynthesis parameters and the parameters related to water and energy across multiple PFTs. In the next work, in order to constrain the water, energy, and carbon fluxes it is recommended to add more sources of observations, such as net ecosystem exchange (NEE) and latent heat (LE), to the various PTFs. Senapati et al. (2016) used data

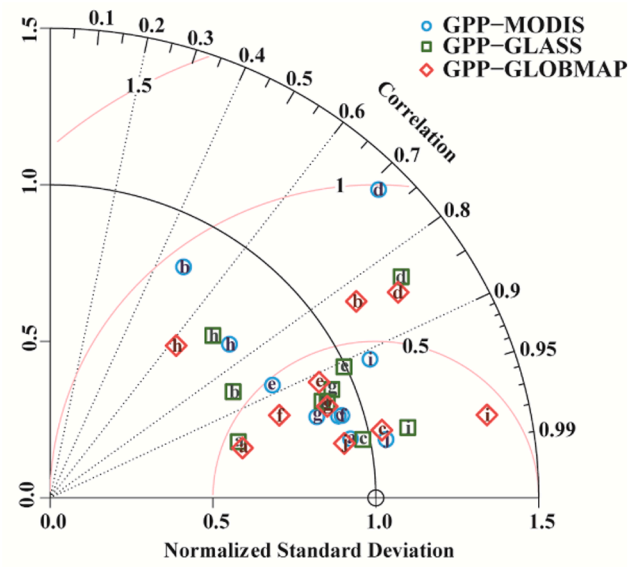

Fig. 9. Comparisons between prior, posterior GPP and observations with monthly GPP (left) and normalized Taylor diagram plot of the GPP simulated with three different LAI products against GPP field measurement plots at 10 sites (right). a, b, c, d, e, f, g, h, i, j at left and right figure represents AR, BN, CB, DHS, DX, HBS, HBW, NMG, QYZ, YK respectively.

from both soil profile observations and eddy covariance measurements to investigate the modeling uncertainty in a grassland area. They also noticed the influences of different observations on model performance in a multi-objective calibration. Metzger et al. (2016) used eddy covariance data and soil profile observations to study uncertainty and equifinality when modeling a peatland ecosystem; and addressed the importance of multiple observations in constraining model performance. For a complex model with strong interactions between different processes, data from soil water, energy and carbon were found all necessary, and they cannot be fully replaced by another (Metzger et al., 2016).

We noticed that some parameter values varied across 10 sites covering 7 PFTs. This indicates that we need to assign parameter values to different ecosystems carefully. Due to the lack of long-term observations from other ecosystems, we drew conclusions based on the 7 plant types from different climate and soil conditions. Since previous studies of optimization typically focused on individual sites for a given PFT (Knorr and Kattge, 2005; Metzger et al., 2016; Wu et al., 2019a), which resulted in parameter values with excessive adjustment to fit a particular site (Kuppel et al., 2014), our study from 10 sites put our understanding of ecosystems forward and made it possible to diagnose the differences in modeling various ecosystems with different environmental conditions. We recommended that it is essential to use observations from a large number of eddy covariance measurement sites to constrain multi-group of parameters to assess the variability of parameter values within and across PFTs (Xiao et al., 2014a) and to get better and more reasonable simulations of GPP over whole China.

5. Conclusions

In this study, we incorporated the Two-Step Global Sensitivity Analysis (TS-GSA) method and the GLUE approach into the ecosystem model BEPS to analyze the sensitivity of GPP to parameter settings and optimize parameters. This implementation was shown efficient to identify the sensitive parameters within the full parameter range using a limited number of simulations. The conclusions are as follows:

(1) We identified that the sensitive parameters in simulating GPP not only come from the photosynthesis process, but also come from the water and energy processes, and we found that different ecosystems exhibited unique sets of sensitive parameters.
(2) We revealed that the parameter uncertainties in simulating GPP were generally well constrained with the GLUE approach, especially the parameter uncertainties of f_{leaf} at the forest sites (BN, CB, DHS, QYZ) and V_{cmax25}, N_{leaf}, and $m_{V_{cmax,N}}$ at shrub HBS, wetland HBW, semi-arid grass NMG and crop YK. The sensitive parameters relevant to different model processes exhibited strong impacts on the model performance at most PFTs, suggesting that the multiple processes need to be carefully considered in order to achieve reasonable simulation results on GPP.
(3) With the constrained parameter sets, we have successfully derived spatial and temporal distributions of the GPP over China with good agreements with other independent datasets. Our results indicated the large GPP over the forest regions in South China.

Generally, we can conclude that in modeling of GPP in different plant functional types, we need to identify parameter sensitivity and reduce parameter uncertainties using a systematic global parameter sensitivity analysis and calibration approach as provided in this study. Since the ecosystem has shown strong couplings between water, energy and carbon cycles, the use of more sites for different PFTs and multiple observations from different processes is necessary in the future.

Data and code availability statement

The eight sites of ChinaFlux are available at http://www.chinaflux.org/enn/index.aspx. The two sites of National Tibetan Plateau Third Pole Environment are available at http://data.tpdc.ac.cn/zh-hans/. The remote-sensing GLOBMAP LAI data are available at https://zenodo.org/record/4700264#.YzvSYnZBxD8/. The remote-sensing GLASS LAI data are available at http://www.bnu-datacenter.com/. The MODIS LAI data are available at http://www.modis.ornl.gov/. The standardized precipitation-evapotranspiration index (SPEI): https://spei.csic.es/index.html. The referenced VPM GPP datasets are available at http://data.tpdc.ac.cn/en/data/582663f5–3be7–4f26-bc45-b56a3c4fc3b7/. The referenced NIRV GPP datasets are available at https://data.tpdc.ac.cn/en/data/d6dff40f-5dbd-4f2d-ac96–55827ab93cc5/. The LRF GPP datasets are available at https://doi.org/10.17894/ucph.b2d7ebfb-c69c-4c97-bee7–562edde5ce66. The EC-LUE GPP datasets are available at https://doi.org/10.6084/m9.figshare.8942336. The software of RS-HDMR method is available upon request from Tilo Ziehn (tilo-ziehn@gmail.com).

CRediT authorship contribution statement

Xiuli Xing: Methodology, Software, Writing – original draft. **Mousong Wu:** Conceptualization, Methodology, Software, Writing – review & editing. **Wenxin Zhang:** Methodology, Writing – review & editing. **Weimin Ju:** Software, Supervision, Writing – review & editing. **Torbern Tagesson:** Data curation, Writing – review & editing. **Wei He:** Data curation, Writing – review & editing. **Songhan Wang:** Data curation, Validation. **Jun Wang:** Software. **Lu Hu:** Visualization. **Shu Yuan:** Investigation. **Tingting Zhu:** Investigation. **Xiaorong Wang:** Validation, Writing – review & editing. **Youhua Ran:** Data curation, Validation. **Sien Li:** Validation. **Chunyu Wang:** Validation. **Fei Jiang:** Funding acquisition, Supervision.

Declaration of Competing Interest

The authors declare that they have no known competing financial interests or personal relationships that could have appeared to influence the work reported in this paper.

Data availability

Data used have been provided with link.

Acknowledgments

This study was supported by the National Natural Science Foundation of China (42141005, 42371486, 42277453, 42111530184, 41901266), the National Key Research and Development Program of China (2020YFA0607504), the Research Funds for the Frontiers Science Center for Critical Earth Material Cycling, Nanjing University (Grant No: 090414380031, 020914380115). Zhang W. acknowledged grant from the Swedish Research Council VR 2020-05338. We thank Tilo Ziehn for providing the RS-HDMR software.

Supplementary materials

Supplementary material associated with this article can be found, in the online version, at doi:10.1016/j.agrformet.2023.109789.

References

Altaf, M.U., El Gharamti, M., Heemink, A.W., Hoteit, I., 2013. A reduced adjoint approach to variational data assimilation. Comput. Methods Appl. Mech. Eng. 254, 1–13.

Ball, J.T., Woodrow, I.E., Berry, J.A., 1987. A model predicting stomatal conductance and its contribution to the control of photosynthesis under different environmental conditions. J. Biggins (Ed.). Progress in Photosynthesis Research: Volume 4 Proceedings of the VIIth International Congress On Photosynthesis Providence, Rhode Island, USA, August 10–15, 1986. Springer Netherlands, Dordrecht, pp. 221–224.

Bastos, A., et al., 2020. Direct and seasonal legacy effects of the 2018 heat wave and drought on European ecosystem productivity. Sci. Adv. 6 (24), eaba2724.

Bastrikov, V., et al., 2018. Land surface model parameter optimisation using *in situ* flux data: comparison of gradient-based versus random search algorithms (a case study using ORCHIDEE v1.9.5.2). Geosci. Model. Dev. 11 (12), 4739–4754.

Beck, M.B., 1987. Water quality modeling: a review of the analysis of uncertainty. Water Resour. Res. 23 (8), 1393–1442.

Beer, C., et al., 2010. Terrestrial gross carbon dioxide uptake: global distribution and covariation with climate. Science 329 (5993), 834–838.

Beven, K., 2006. A manifesto for the equifinality thesis. J. Hydrol. 320 (1–2), 18–36.

Beven, K., 2009. Environmental Modelling: an Uncertain future?: an Introduction to Techniques For Uncertainty Estimation in Environmental Prediction. Routledge, London.

Beven, K., Binley, A., 1992. The future of distributed models: model calibration and uncertainty prediction. Hydrol. Process. 6 (3), 279–298.

Beven, K., Freer, J., 2001. Equifinality, data assimilation, and uncertainty estimation in mechanistic modelling of complex environmental systems using the GLUE methodology. J. Hydrol. 249 (1–4), 11–29.

Bonan, G.B., Pollard, D., Thompson, S.L., 1993. Influence of subgrid-scale heterogeneity in leaf area index, stomatal resistance, and soil moisture on grid-scale land–atmosphere interactions. J. Clim. 6 (10), 1882–1897.

Castaings, W., Borgonovo, E., Morris, M.D., Tarantola, S., 2012. Sampling strategies in density-based sensitivity analysis. Environ. Model. Softw. 38, 13–26.

Chen, B., Chen, J.M., Ju, W., 2007. Remote sensing-based ecosystem–atmosphere simulation scheme (EASS)—Model formulation and test with multiple-year data. Ecol. Model. 209 (2–4), 277–300.

Chen, J.M., et al., 2019a. Vegetation structural change since 1981 significantly enhanced the terrestrial carbon sink. Nat. Commun. 10 (1), 4259.

Chen, J.M., et al., 2019b. Vegetation structural change since 1981 significantly enhanced the terrestrial carbon sink. Nat. Commun. 10 (1), 4265.

Chen, J.M., Liu, J., Cihlar, J., Goulden, M.L., 1999. Daily canopy photosynthesis model through temporal and spatial scaling for remote sensing applications. Ecol. Model. 124 (2), 99–119.

Chen, Z., et al., 2017. Optimization of terrestrial ecosystem model parameters using atmospheric CO_2 concentration data with the global carbon assimilation system (GCAS). J. Geophys. Res. Biogeosci. 122 (12), 3218–3237.

Cheng, G., Wu, T., 2007. Responses of permafrost to climate change and their environmental significance, Qinghai-Tibet Plateau. J. Geophys. Res. 112 (F2), F02S03.

Czitrom, V., 1999. One-factor-at-a-time versus designed experiments. Am. Stat. 53 (2), 126–131.

Dagon, K., Sanderson, B.M., Fisher, R.A., Lawrence, D.M., 2020. A machine learning approach to emulation and biophysical parameter estimation with the Community Land Model, version 5. Adv. Stat. Clim. Meteorol. Oceanogr. 6 (2), 223–244.

Dantec-Nédélec, S., et al., 2017. Testing the capability of ORCHIDEEland surface model to simulateArctic ecosystems: sensitivity analysis and site-level model calibration. J. Adv. Model. Earth Syst. 9 (2), 1212–1230.

Elbern, H., Schmidt, H., Talagrand, O., Ebel, A., 2000. 4D-variational data assimilation with an adjoint air quality model for emission analysis. Environ. Model. Softw. 15 (6), 539–548.

Fang, H., Wei, S., Jiang, C., Scipal, K., 2012. Theoretical uncertainty analysis of global MODIS, CYCLOPES, and GLOBCARBON LAI products using a triple collocation method. Remote Sens. Environ. 124, 610–621.

Farquhar, G.D., von Caemmerer, S., Berry, J.A., 1980. A biochemical model of photosynthetic CO_2 assimilation in leaves of C_3 species. Planta 149 (1), 78–90.

Forkel, M., et al., 2016. Enhanced seasonal CO_2 exchange caused by amplified plant productivity in northern ecosystems. Science 351 (6274), 696–699.

Franks, S.W., Beven, K.J., Quinn, P.F., Wright, I.R., 1997. On the sensitivity of soil-vegetation-atmosphere transfer (SVAT) schemes: equifinality and the problem of robust calibration. Agric. For. Meteorol. 86 (1–2), 63–75.

Gampe, D., et al., 2021. Increasing impact of warm droughts on northern ecosystem productivity over recent decades. Nat. Clim. Change 11 (9), 772–779.

He, Q., et al., 2021. Drought risk of global terrestrial gross primary productivity over the last 40 years detected by a remote sensing-driven process model. J. Geophys. Res. Biogeosci. 126 (6), e2020JG005944.

He, L., Chen, J.M., Liu, J., Bélair, S., Luo, X., 2017. Assessment of SMAP soil moisture for global simulation of gross primary production. J. Geophys. Res. Biogeosci. 122 (7), 1549–1563.

Hatfield, S., et al., 2021. Building tangent-linear and adjoint models for data assimilation with neural networks. J. Adv. Model. Earth Syst. 13 (9), e2021MS002521.

He, L., et al., 2014. Optimization of water uptake and photosynthetic parameters in an ecosystem model using tower flux data. Ecol. Model. 294, 94–104.

Hersbach, H., et al., 2020. The ERA5 global reanalysis. Q. J. R. Meteorolog. Soc. 146 (730), 1999–2049.

Houska, T., Multsch, S., Kraft, P., Frede, H.G., Breuer, L., 2014. Monte Carlo-based calibration and uncertainty analysis of a coupled plant growth and hydrological model. Biogeosciences 11 (7), 2069–2082.

Huang, X., Xiao, J., Wang, X., Ma, M., 2021. Improving the global MODIS GPP model by optimizing parameters with FLUXNET data. Agric. For. Meteorol. 300, 108314.

Huntzinger, D.N., et al., 2017. Uncertainty in the response of terrestrial carbon sink to environmental drivers undermines carbon-climate feedback predictions. Sci. Rep. 7 (1), 4765.

Jabloun, M., et al., 2018. Sensitivity of simulated crop yield and nitrate leaching of the wheat-maize cropping system in the North China Plain to model parameters. Agric. For. Meteorol. 263, 25–40.

Jansson, P.E., 2012. CoupModel: model use, calibration, and validation. Trans. ASABE 55 (4), 1337.

Ju, W., et al., 2006. Modelling multi-year coupled carbon and water fluxes in a boreal aspen forest. Agric. For. Meteorol. 140 (1–4), 136–151.

Ju, W., Wang, S., Yu, G., Zhou, Y., Wang, H., 2010. Modeling the impact of drought on canopy carbon and water fluxes for a subtropical evergreen coniferous plantation in southern China through parameter optimization using an ensemble Kalman filter. Biogeosciences 7 (3), 845–857.

Kaminski, T., et al., 2013. The BETHY/JSBACH carbon cycle data assimilation system: experiences and challenges. J. Geophys. Res. Biogeosci. 118 (4), 1414–1426.

Khoshkhoo, Y., Jansson, P.E., Irannejad, P., Khalili, A., Rahimi, H., 2015. Calibration of an energy balance model to simulate wintertime soil temperature, soil frost depth, and snow depth for a 14 year period in a highland area of Iran. Cold Reg. Sci. Technol. 119, 47–60.

Knorr, W., Kattge, J., 2005. Inversion of terrestrial ecosystem model parameter values against eddy covariance measurements by Monte Carlo sampling. Glob. Change Biol. 11 (8), 1333–1351.

Koppa, A., Rains, D., Hulsman, P., Poyatos, R., Miralles, D.G., 2022. A deep learning-based hybrid model of global terrestrial evaporation. Nat. Commun. 13 (1), 1912.

Kuppel, S., et al., 2014. Model–data fusion across ecosystems: from multisite optimizations to global simulations. Geosci. Model. Dev. 7 (6), 2581–2597.

Li, X., et al., 2013. Heihe watershed allied telemetry experimental research (HiWATER): scientific objectives and experimental design. Bull. Am. Meteorol. Soc. 94 (8), 1145–1160.

Li, X., Xiao, J., He, B., 2018. Higher absorbed solar radiation partly offset the negative effects of water stress on the photosynthesis of Amazon forests during the 2015 drought. Environ. Res. Lett. 13 (4), 044005.

Liu, D., et al., 2018a. Contrasting responses of grassland water and carbon exchanges to climate change between Tibetan Plateau and Inner Mongolia. Agric. For. Meteorol. 249, 163–175.

Liu, X., et al., 2022. Plant drought tolerance trait is the key parameter in improving the modeling of terrestrial transpiration in arid and semi-arid regions. Atmos. Ocean. Sci. Lett. 15 (1), 100139.

Li, X., et al., 2009. Watershed Allied Telemetry Experimental Research. J. Geophys. Res. 114 (D22), D22103.

Li, J., et al., 2020. Quantifying contributions of uncertainties in physical parameterization schemes and model parameters to overall errors in Noah-MP dynamic vegetation modeling. J. Adv. Model. Earth Syst. 12 (7) e2019MS001914.

Liu, Y., Liu, R., Chen, J.M., 2012. Retrospective retrieval of long-term consistent global leaf area index (1981-2011) from combined AVHRR and MODIS data. J. Geophys. Res. Biogeosci. 117 (G4), G04003.

Liu, Y., et al., 2018b. Satellite-derived LAI products exhibit large discrepancies and can lead to substantial uncertainty in simulated carbon and water fluxes. Remote Sens. Environ. 206, 174–188.

Lu, X., Wang, Y.P., Ziehn, T., Dai, Y., 2013. An efficient method for global parameter sensitivity analysis and its applications to the Australian community land surface model (CABLE). Agric. For. Meteorol. 182-183, 292–303.

Luo, Y., Weng, E., Wu, X., Gao, C., Zhou, X., Li, Z., 2009. Parameter identifiability, constraint, and equifinality in data assimilation with ecosystem models. Ecol. Appl. 19 (3), 571–574.
Ma, R., et al., 2022. Spatial parameter optimization of a terrestrial biosphere model for improving estimation of carbon fluxes for deciduous forests in the eastern United States: an efficient model-data fusion method. Geosci. Model Dev. Discuss. 2022, 1–35.
MacBean, N., et al., 2022. Quantifying and reducing uncertainty in global carbon cycle predictions: lessons and perspectives from 15 Years of data assimilation studies with the ORCHIDEE terrestrial biosphere model. Glob. Biogeochem. Cycles 36 (7) e2021GB007177.
Massad, R.S., Tuzet, A., Bethenod, O., 2007. The effect of temperature on C(4)-type leaf photosynthesis parameters. Plant Cell Environ. 30 (9), 1191–1204.
Maxwell, R.M., Condon, L.E., 2016. Connections between groundwater flow and transpiration partitioning. Science 353 (6297), 377–380.
Metropolis, N., Ulam, S., 1949. The monte carlo method. J. Am. Stat. Assoc. 44 (247), 335–341.
Metzger, C., Nilsson, M.B., Peichl, M., Jansson, P.E., 2016. Parameter interactions and sensitivity analysis for modelling carbon heat and water fluxes in a natural peatland, using CoupModel v5. Geosci. Model. Dev. 9 (12), 4313–4338.
Migliavacca, M., et al., 2021. The three major axes of terrestrial ecosystem function. Nature 598 (7881), 468–472.
Mo, X., Chen, J.M., Ju, W., Black, T.A., 2008. Optimization of ecosystem model parameters through assimilating eddy covariance flux data with an ensemble Kalman filter. Ecol. Model. 217 (1–2), 157–173.
Morris, M.D., 1991. Factorial sampling plans for preliminary computational experiments. Technometrics 33 (2), 161–174.
Norton, J., 2015. An introduction to sensitivity assessment of simulation models. Environ. Model. Softw. 69, 166–174.
O'Neill, R.V., Gardner, R.H., Carney, J.H., 1982. Parameter constraints in a stream ecosystem model: incorporation of a priori information in Monte Carlo error analysis. Ecol. Model. 16 (1), 51–65.
Orth, R., Destouni, G., Jung, M., Reichstein, M., 2020. Large-scale biospheric drought response intensifies linearly with drought duration in arid regions. Biogeosciences 17 (9), 2647–2656.
Pianosi, F., Sarrazin, F., Wagener, T., 2015. A Matlab toolbox for global sensitivity analysis. Environ. Model. Softw. 70, 80–85.
Piao, S., et al., 2013. Evaluation of terrestrial carbon cycle models for their response to climate variability and to CO_2 trends. Glob. Change Biol. 19 (7), 2117–2132.
Prihodko, L., Denning, A.S., Hanan, N.P., Baker, I., Davis, K., 2008. Sensitivity, uncertainty and time dependence of parameters in a complex land surface model. Agric. For. Meteorol. 148 (2), 268–287.
Qiu, J., 2010. China drought highlights future climate threats: yunnan's worst drought for many years has been exacerbated by destruction of forest cover and a history of poor water management. Nature 465 (7295), 142–144.
Rayner, P.J., et al., 2005. Two decades of terrestrial carbon fluxes from a carbon cycle data assimilation system (CCDAS). Glob. Biogeochem. Cycles 19 (2), GB2026.
Richardson, A.D., et al., 2012. Terrestrial biosphere models need better representation of vegetation phenology: results from the North American Carbon Program Site Synthesis. Glob. Change Biol. 18 (2), 566–584.
Running, S.W., et al., 2004. A continuous satellite-derived measure of global terrestrial primary production. Bioscience 54 (6), 547–560.
Sawada, Y., 2020. Machine learning accelerates parameter optimization and uncertainty assessment of a land surface model. J. Geophys. Res.: Atmos. 125 (20), e2020JD032688.
Scholze, M., et al., 2016. Simultaneous assimilation of SMOS soil moisture and atmospheric CO_2 *in-situ* observations to constrain the global terrestrial carbon cycle. Remote Sens. Environ. 180, 334–345.
Scholze, M., et al., 2019. Mean European carbon sink over 2010–2015 estimated by simultaneous assimilation of atmospheric CO_2, soil moisture, and vegetation optical depth. Geophys. Res. Lett. 46 (23), 13796–13803.
Seddon, A.W., Macias-Fauria, M., Long, P.R., Benz, D., Willis, K.J., 2016. Sensitivity of global terrestrial ecosystems to climate variability. Nature 531 (7593), 229–232.
Senapati, N., Jansson, P.E., Smith, P., Chabbi, A., 2016. Modelling heat, water and carbon fluxes in mown grassland under multi-objective and multi-criteria constraints. Environ. Model. Softw. 80, 201–224.
Sitch, S., et al., 2015. Recent trends and drivers of regional sources and sinks of carbon dioxide. Biogeosciences 12 (3), 653–679.
Sobol, I.M., 1993. Sensitivity analysis for non-linear mathematical models. Mathematical Modelling and Computational Experiments 4, 407–414.
Stedinger, J.R., Vogel, R.M., Lee, S.U., Batchelder, R., 2008. Appraisal of the generalized likelihood uncertainty estimation (GLUE) method. Water Resour. Res. 44 (12), W00B06.
Tagesson, T., et al., 2021. A physiology-based earth observation model indicates stagnation in the global gross primary production during recent decades. Glob. Change Biol. 27 (4), 836–854.
Tarantola, S., Gatelli, D., Mara, T.A., 2006. Random balance designs for the estimation of first order global sensitivity indices. Reliab. Eng. Syst. Saf. 91 (6), 717–727.
Trugman, A.T., Medvigy, D., Mankin, J.S., Anderegg, W.R.L., 2018. Soil moisture stress as a major driver of carbon cycle uncertainty. Geophys. Res. Lett. 45 (13), 6495–6503.
Verbeeck, H., Samson, R., Verdonck, F., Lemeur, R., 2006. Parameter sensitivity and uncertainty of the forest carbon flux model FORUG: a Monte Carlo analysis. Tree Physiol. 26 (6), 807–817.
Vicente-Serrano, S.M., et al., 2013. Response of vegetation to drought time-scales across global land biomes. Proc. Natl. Acad. Sci. U. S. A. 110 (1), 52–57.
Wang, C., et al., 2022a. Modelling water and energy fluxes with an explicit representation of irrigation under mulch in a maize field. Agric. For. Meteorol. 326, 109145.
Wang, J., et al., 2021a. Constraining global terrestrial gross primary productivity in a global carbon assimilation system with OCO-2 chlorophyll fluorescence data. Agric. For. Meteorol. 304–305.
Wang, J., Li, X., Lu, L., Fang, F., 2013. Parameter sensitivity analysis of crop growth models based on the extended Fourier Amplitude Sensitivity Test method. Environ. Model. Softw. 48, 171–182.
Wang, S., et al., 2020. Recent global decline of CO_2 fertilization effects on vegetation photosynthesis. Science 370 (6522), 1295–1300.
Wang, S., Zhang, Y., Ju, W., Qiu, B., Zhang, Z., 2021b. Tracking the seasonal and inter-annual variations of global gross primary production during last four decades using satellite near-infrared reflectance data. Sci. Total Environ. 755 (Pt 2), 142569.
Wang, S., et al., 2022b. Temporally corrected long-term satellite solar-induced fluorescence leads to improved estimation of global trends in vegetation photosynthesis during 1995–2018. ISPRS J. Photogramm. Remote Sens. 194, 222–234.
Wang, X., Qiu, B., Li, W., Zhang, Q., 2019. Impacts of drought and heatwave on the terrestrial ecosystem in China as revealed by satellite solar-induced chlorophyll fluorescence. Sci. Total Environ. 693, 133627.
Wenzel, S., Cox, P.M., Eyring, V., Friedlingstein, P., 2016. Projected land photosynthesis constrained by changes in the seasonal cycle of atmospheric CO_2. Nature 538 (7626), 499–501.
Wu, M., et al., 2019a. Global parameters sensitivity analysis of modeling water, energy and carbon exchange of an arid agricultural ecosystem. Agric. For. Meteorol. 271, 295–306.
Wu, M., Scholze, M., Kaminski, T., Voßbeck, M., Tagesson, T., 2020a. Using SMOS soil moisture data combining CO_2 flask samples to constrain carbon fluxes during 2010–2015 within a Carbon Cycle Data Assimilation System (CCDAS). Remote Sens. Environ. 240, 111719.
Wu, M., Scholze, M., Voßbeck, M., Kaminski, T., Hoffmann, G., 2019b. Simultaneous assimilation of remotely sensed soil moisture and FAPAR for improving terrestrial carbon fluxes at multiple sites using CCDAS. Remote Sens. 11 (1), 27.
Wu, M., et al., 2020b. Coupled water transport and heat flux in seasonally frozen soils: uncertainties identification in multi-site calibration. Environ. Earth Sci. 79 (23), 1–21.
Wu, M., et al., 2019c. Simulation of dynamical interactions between soil freezing/thawing and salinization for improving water management in cold/arid agricultural region. Geoderma 338, 325–342.
Wu, M., et al., 2021. Improved soil hydrological modeling with the implementation of salt-induced freezing point depression in CoupModel: model calibration and validation. J. Hydrol. 596, 125693.
Wu, S.H., Jansson, P.E., Kolari, P., 2011. Modeling seasonal course of carbon fluxes and evapotranspiration in response to low temperature and moisture in a boreal Scots pine ecosystem. Ecol. Model. 222 (17), 3103–3119.
Wu, S.H., Jansson, P.E., Kolari, P., 2012. The role of air and soil temperature in the seasonality of photosynthesis and transpiration in a boreal Scots pine ecosystem. Agric. For. Meteorol. 156, 85–103.
Xiao, J., Davis, K.J., Urban, N.M., Keller, K., 2014a. Uncertainty in model parameters and regional carbon fluxes: a model-data fusion approach. Agric. For. Meteorol. 189-190, 175–186.
Xiao, J., et al., 2014b. Data-driven diagnostics of terrestrial carbon dynamics over North America. Agric. For. Meteorol. 197, 142–157.
Xie, X., et al., 2019. Assessment of five satellite-derived LAI datasets for GPP estimations through ecosystem models. Sci. Total Environ. 690, 1120–1130.
Xu, X., Medvigy, D., Powers, J.S., Becknell, J.M., Guan, K., 2016. Diversity in plant hydraulic traits explains seasonal and inter-annual variations of vegetation dynamics in seasonally dry tropical forests. New Phytol. 212 (1), 80–95.
Yang, Y., et al., 2022. CARDAMOM-FluxVal version 1.0: a FLUXNET-based validation system for CARDAMOM carbon and water flux estimates. Geosci. Model. Dev. 15 (4), 1789–1802.
Zhang, W., et al., 2019. Model-data fusion to assess year-round CO2 fluxes for an arctic heath ecosystem in West Greenland (69°N). Agric. For. Meteorol. 272-273, 176–186.
Zhang, Y., et al., 2017. A global moderate resolution dataset of gross primary production of vegetation for 2000-2016. Sci. Data 4, 170165.
Zheng, Y., et al., 2020. Improved estimate of global gross primary production for reproducing its long-term variation, 1982-2017. Earth Syst. Sci. Data 12 (4), 2725–2746.
Zheng, Y., et al., 2018. Sources of uncertainty in gross primary productivity simulated by light use efficiency models: model structure, parameters, input data, and spatial resolution. Agric. For. Meteorol. 263, 242–257.
Zhou, S., Duursma, R.A., Medlyn, B.E., Kelly, J.W.G., Prentice, I.C., 2013. How should we model plant responses to drought? An analysis of stomatal and non-stomatal responses to water stress. Agric. For. Meteorol. 182-183, 204–214.
Zhu, L., Chen, J.M., Qin, Q., Li, J., Wang, L., 2009. Optimization of ecosystem model parameters using spatio-temporal soil moisture information. Ecol. Model. 220 (18), 2121–2136.
Zhu, Q., Zhuang, Q., 2014. Parameterization and sensitivity analysis of a process-based terrestrial ecosystem model using adjoint method. J. Adv. Model. Earth Syst. 6 (2), 315–331.
Ziehn, T., Tomlin, A.S., 2008. A global sensitivity study of sulfur chemistry in a premixed methane flame model using HDMR. Int. J. Chem. Kinet. 40 (11), 742–753.
Ziehn, T., Tomlin, A.S., 2009. GUI–HDMR – A software tool for global sensitivity analysis of complex models. Environ. Model. Softw. 24 (7), 775–785.